Catalysis Science & Technology

PAPER

View Article Online
View Journal | View Issue

Cite this: *Catal. Sci. Technol.*, 2014, **4**, 1144

Hydrothermal synthesis of zinc indium sulfide microspheres with Ag^+ doping for enhanced H_2 production by photocatalytic water splitting under visible light†

Fan Li,[a] Jianheng Luo,[a] Guoping Chen,[a] Yuzun Fan,[b] Qingli Huang,[a] Yanhong Luo,[a] Dongmei Li*[a] and Qingbo Meng*[a]

Received 21st November 2013,
Accepted 24th December 2013

DOI: 10.1039/c3cy00952a

www.rsc.org/catalysis

Two series of $ZnIn_xS_{1+1.5x}$ and Ag(y)–$ZnIn_xS_{1+1.5x+0.5y}$ solid solutions are prepared by hydrothermal methods. The synthetic conditions such as the molar ratio of In/Zn, the pH value, the hydrothermal temperature and the reaction time are found to intensely influence the crystal structure and the morphology of the photocatalyst as well as its photocatalytic activity for H_2 generation from water. It is revealed that the $ZnIn_{1.5}S_{3.25}$ solid solution (In/Zn = 1.5) prepared at 160 °C for 6 h by adding 1 mL hydrochloric acid to the precursor solution shows the highest photocatalytic H_2 evolution rate of 1.85 mmol h^{-1} g^{-1} in the presence of Ru as the co-catalyst and Na_2S/Na_2SO_3 as sacrificial reagents. Furthermore, after Ag^+ doping, the photocatalytic H_2 evolution rate remarkably increased to 3.20 mmol h^{-1} g^{-1} for the Ag(1.5%)–$ZnIn_{1.5}S_{3.2575}$ sample. This work provides a new opportunity to develop efficient photocatalysts for photosplitting water into hydrogen.

Introduction

Since the Honda–Fujishima effect of water splitting on a TiO_2 electrode was discovered in 1972, photocatalytic hydrogen production from water has attracted worldwide interest.[1,2] To realize highly efficient water photosplitting into hydrogen, much effort has been focused on developing various photocatalysts, especially with visible-light response, because visible light constitutes 43% of the solar energy.[3–5] In recent years, inorganic semiconductor CdS has been developed as a promising visible-light-driven photocatalyst due to its narrow band gap and high absorption coefficient.[6–8] However, pure CdS exhibits extremely low photocatalytic activity and suffers photocorrosion during photoreactions as well.[9] Tremendous efforts have been devoted to solve the above problems, such as co-catalyst loading,[8,10–13] forming junctions between CdS and another semiconductor,[14,15] loading CdS nanoparticles on mesoporous materials,[16,17] *etc.* Recently, Li and co-workers reported Pt-PdS/CdS with the highest apparent quantum efficiency of 93% for photocatalytic water splitting into hydrogen.[8] However, the practical application of CdS photocatalysts will be limited by environmental contamination.[9] Therefore, it is necessary to design and synthesize more stable and environmentally friendly photocatalysts.

Ternary Zn–In–S solid solutions with the stoichiometric ratio Zn : In : S = 1 : 2 : 4 have been widely investigated as potential eco-friendly visible-light-driven photocatalysts with relatively low toxicity.[18–23] Li and co-workers firstly reported that $ZnIn_2S_4$ can exhibit a steady photocatalytic activity for water splitting to H_2 over 150 hours.[18] Li and Bai synthesized hexagonal $ZnIn_2S_4$ porous microspheres with a high specific surface area of 165.4 m^2 g^{-1} through a CPBr-assisted hydrothermal method, which showed 1544.8 μmol h^{-1} g^{-1} of H_2 evolution rate.[24] Li and Chen synthesized cubic $ZnIn_2S_4$ nanoparticles and hexagonal $ZnIn_2S_4$ flower-like microspheres *via* a facile hydrothermal method by changing the metal precursors and found that the cubic phase can achieve better photocatalytic activity than the hexagonal phase.[25] Qian and co-workers found that the increase in {006} facets of hexagonal $ZnIn_2S_4$, terminated by metal ions, can improve the photocatalytic H_2 evolution rate to 220.45 μmol h^{-1}.[26] Guo's group synthesized Cu^{2+} and Ni^{2+} doped $ZnIn_2S_4$ microspheres *via* hydrothermal processes, whose photocatalytic

[a] *Key Laboratory for Renewable Energy, Beijing Key Laboratory for New Energy Materials and Devices, Beijing National Laboratory for Condense Matter Physics, Institute of Physics, Chinese Academy of Sciences, Beijing, China. E-mail: qbmeng@iphy.ac.cn, dmli@iphy.ac.cn; Fax: +86 10 82649242; Tel: +86 10 82649242*

[b] *Key Laboratory of Bio-Inspired Smart Interfacial Science and Technology of Ministry of Education, Beijing Key Laboratory of Bio-inspired Energy Materials and Devices, School of Chemistry and Environment, Beihang University, Beijing 100191, PR China*

† Electronic supplementary information (ESI) available: More information of XRD patterns, SEM images, X-ray energy dispersive spectroscopy (XEDS) maps and XPS characterization. See DOI: 10.1039/c3cy00952a

activities were much higher than that of the un-doped $ZnIn_2S_4$.[27,28] However, few studies have been reported about the influence of different In/Zn ratios and other transition metal ion doping (such as Ag^+) on the photocatalytic properties of the Zn–In–S solid solution.

Herein, a Zn–In–S solid solution (labeled as $ZnIn_xS_{1+1.5x}$) and a Ag^+ doped Zn–In–S solid solution (labeled as Ag(y)–$ZnIn_xS_{1+1.5x+0.5y}$) were prepared by hydrothermal methods. The photocatalytic activities of the two series of photocatalysts for water splitting into hydrogen are evaluated under visible-light illumination in the presence of Na_2S/Na_2SO_3 as sacrificial reagents and Ru as the co-catalyst. The synthetic conditions such as the molar ratio of In/Zn, the pH value, the hydrothermal temperature and the reaction time were systematically studied to investigate their influence on the morphologies of the photocatalysts and the photocatalytic activities for hydrogen evolution. Besides, after Ag^+ doping, the photocatalytic H_2 evolution rate remarkably improved to 3.20 mmol h^{-1} g^{-1} for the Ag(1.5%)–$ZnIn_{1.5}S_{3.2575}$ solid solution, in comparison to 1.85 mmol h^{-1} g^{-1} for the corresponding $ZnIn_{1.5}S_{3.25}$ solid solution.

Experimental

Reagents and chemicals

All of the reagents were used without further purification. Silver nitrate ($AgNO_3$, AR, 99.8%), $Na_2S{\cdot}9H_2O$ (AR, 98%) and Na_2SO_3 (AR, 97%) were from Xilonghuagong, indium nitrate ($In(NO_3)_3{\cdot}4.5H_2O$, 99.5%), zinc nitrate ($Zn(NO_3)_2{\cdot}6H_2O$, AR, 99%), thioacetamide (C_2H_5NS, AR, 99%) and $RuCl_3{\cdot}xH_2O$ (at least 37 wt% Ru) from Sinopharm.

Synthesis of $ZnIn_xS_{1+1.5x}$ and Ag(y)–$ZnIn_xS_{1+1.5x+0.5y}$ solid solution samples

In a typical synthesis of $ZnIn_xS_{1+1.5x}$ solid solution samples, 30 mL of a metal nitrate aqueous solution with different In/Zn molar ratios (here, $Zn(NO_3)_2{\cdot}6H_2O$ was fixed at 1 mmol) and a double excess of thioacetamide were stirred rigorously to form a homogeneous solution. The pH value of the mixed solution was adjusted using different amounts of hydrochloric acid (12 mol L^{-1}), which were in the range of 0–3 mL. The mixed solution was then transferred into a 45 mL Teflon-lined autoclave. The autoclave was sealed and maintained at 160 °C for 6 hours. After cooling down to room temperature, the reaction mixture was centrifuged to give the precipitate, which was washed with deionized water and ethanol several times, collected and dried in a vacuum oven overnight. For the doped solid solution, a tiny amount of $AgNO_3$ was added together with In^{3+} and Zn^{2+} into the precursor solution before the hydrothermal reaction. The doping percentage of Ag^+ is defined as the molar ratio of $Ag^+/(In^{3+}+Zn^{2+})$ in the precursor solution, which was in the range of 0–3%.

Characterization

The X-ray diffraction patterns (XRD) of the samples were obtained using a Bruker D8 Advance X-ray diffractometer with Cu-Kα irradiation (λ = 0.154178 nm) at 40 kV and 40 mA. The scan rate is 0.1° s^{-1}. The surface morphologies of the samples were investigated using a scanning electron microscope (SEM, XL30 S-FEG, FEI). The UV-visible diffuse reflectance spectra (UV-vis DRS) were obtained on a UV-visible spectrophotometer (UV-2450, Shimadzu) and were converted from reflectance to absorbance by the Kubelka–Munk method. X-ray photoelectron spectroscopy data (XPS) were collected on an AXIS ULTRA^{DLD} system with an Al Kα chromatic X-ray source (1486.6 eV). All binding energies were referenced to the C1s peak of 284.8 eV.

Photocatalytic activity measurement

The photocatalytic reactions were carried out in a Pyrex reaction cell connected to a homemade closed gas circulation and an evacuation system. 0.1 g of the photocatalyst powder was ultrasonically dispersed for 10 min in a 100 mL aqueous solution containing 0.35 M Na_2S and 0.25 M Na_2SO_3 as sacrificial reagents. Then the suspension was thoroughly degassed and irradiated by a 300 W Xe lamp (PLS-SXE300, Trusttech) equipped with an optical filter ($\lambda \geq 420$ nm) to cut off ultraviolet light and a water filter to remove infrared light. The Ru co-catalyst was *in situ* deposited according to the reference, that is, the reaction mixture with 0.5 wt% of $RuCl_3{\cdot}xH_2O$ (metal basis) was irradiated under an Xe lamp with a full spectrum for 30 min before the H_2 production measurement.[29] The evolved H_2 amount was determined by an on-line gas chromatography with a thermal conductivity detector (Varian, CP3800, molecular sieve 5 Å column, Ar carrier). The photocatalytic activities were compared using the average H_2 evolution rate in the first 5 hours.

Results and discussion

XRD patterns of $ZnIn_xS_{1+1.5x}$ solid solution samples with different molar ratios and Ag(y)–$ZnIn_{1.5}S_{3.25+0.5y}$ samples with different doping amounts

Fig. 1 shows the X-ray diffraction patterns of the $ZnIn_xS_{1+1.5x}$ samples with different In/Zn compositions, whose preparation conditions include using 1 mL hydrochloric acid to

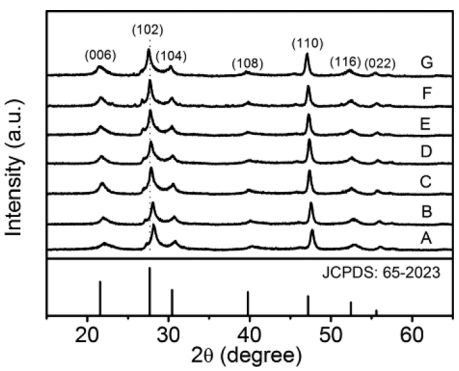

Fig. 1 XRD patterns of $ZnIn_xS_{1+1.5x}$ solid solution samples prepared by adding 1 mL hydrochloric acid at 160 °C for 6 h. The x values of the samples are (A) 0.8; (B) 1.0; (C) 1.2; (D) 1.5; (E) 1.8; (F) 2.0; (G) 3.0.

adjust the pH value and then hydrothermal reaction at 160 °C for 6 hours. It is found that the single phase of a hexagonal structure (JCPDS: 65-2023) is obtained for all the samples, which is in agreement with the literature.[25,30] With the value of x increasing, the (102) diffraction peak shows a successive shift to lower angle, indicating that the samples are the $ZnIn_xS_{1+1.5x}$ solid solution, instead of a simple mixture of In_2S_3 and ZnS. Similar diffraction patterns were reported in previous work about ternary or multinary sulfide systems.[31,32] The influence of different amounts of hydrochloric acid in the preparation process on the composition of $ZnIn_{1.5}S_{3.25}$ is also investigated (Fig. S1†). It can be seen that when no extra hydrochloric acid was added, the diffraction patterns can be indexed to a cubic phase (JCPDS: 48-1778). When 0.25 and 0.5 mL of hydrochloric acid were added, respectively, the hexagonal phase (JCPDS: 65-2023) appears with a relatively low crystallinity, and the solid solutions are indeed the mixture of the two structures. Upon further increasing the amount of hydrochloric acid to 1 mL, the pure hexagonal phase is obtained (plot D in Fig. S1†). However, when 1.5 mL or more were added, the unexpected crystal phase of sulfur was observed (marked diffraction peaks in Fig. S1†), which is supposed to be disadvantageous to the photocatalytic activities (discussed below). Obviously, hydrochloric acid significantly influences the crystal structures of the $ZnIn_xS_{1+1.5x}$ solid solution, which is in agreement with Li and Chen's work.[25]

Fig. 2 illustrates the XRD patterns of Ag^+ doped samples. No distinct changes for the position of the diffraction peaks are found with the variation of the doping amount. In spite of the ionic size of Ag^+ (1.14 Å) being much larger than that of Zn^{2+} (0.74 Å) and In^{3+} (0.76 Å), however, the doping amount is too little to influence the position of the diffraction peaks significantly.[33]

SEM images of $ZnIn_{1.5}S_{3.25}$ solid solution samples prepared using different amounts of hydrochloric acid and Ag(y)–$ZnIn_{1.5}S_{3.25+0.5y}$ samples with different doping amounts

The morphologies of $ZnIn_{1.5}S_{3.25}$ solid solution samples with different amounts of hydrochloric acid added are investigated, as shown in Fig. 3. The morphologies are significantly different upon adding different amounts of hydrochloric acid. Without using hydrochloric acid, the morphology of the $ZnIn_{1.5}S_{3.25}$ samples can be described as microparticles with irregular shapes (Fig. 3a). It is interesting that $ZnIn_{1.5}S_{3.25}$ samples with adding 0.25 and 0.5 mL hydrochloric acid show a transitional form in their morphologies. The surface of the microsphere is composed of plate-like hierarchical structures. Upon adding 1 mL hydrochloric acid before the hydrothermal reaction, the microspheres obtained develop totally plate-like hierarchical structures about 5 μm in size. However, these integrated structures are broken when more hydrochloric acid is used. These changes in the morphologies are consistent with the XRD results, indicating that using different amounts of hydrochloric acid indeed has a significant influence on the crystal structure and morphology of the solid solution samples. Besides, the morphologies of the $ZnIn_{1.5}S_{3.25}$ samples prepared at different hydrothermal temperatures and reaction times at 160 °C with 1 mL hydrochloric acid added are investigated by SEM (images shown in Fig. S2†). It is found that the morphologies of the samples prepared at different hydrothermal temperatures are similar except for the broken plate-like hierarchical microspheres for the sample hydrothermally treated at 200 °C (shown in Fig. S2e†). A hollow structure is thus suggested from the broken microsphere. Furthermore, the morphologies of the $ZnIn_{1.5}S_{3.25}$ samples prepared for 9 h show a more disordered structure than the other two samples, as shown in Fig. S3,† which may be the reason for the lower photocatalytic H_2 evolution rate in comparison to the samples hydrothermally treated for 3 h and 6 h. Moreover, Fig. 4 shows the change of morphologies by varying the doping amount of Ag(y)–$ZnIn_{1.5}S_{3.25+0.5y}$ samples. It is found that the morphologies of the samples prepared with different doping amounts are all plate-like hierarchical microspheres without distinct differences.

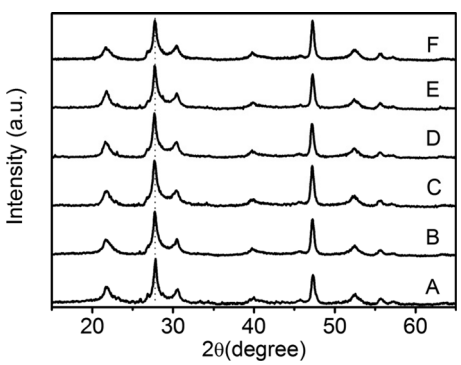

Fig. 2 XRD patterns of Ag(y)–$ZnIn_{1.5}S_{3.25+0.5y}$ solid solution samples prepared with different Ag^+ doping amounts at 160 °C for 6 h and with 1 mL hydrochloric acid added. The Ag^+ doping amounts are (A) 0; (B) 0.5%; (C) 1.0%; (D) 1.5%; (E) 2.0%; (F) 3.0%. Plot A is the same as plot D in Fig. 1.

UV-vis diffuse reflectance spectra of Ag(y)–$ZnIn_{1.5}S_{3.25+0.5y}$ samples with different doping amounts

As we know, transition metal ion doping can enhance charge transfer and photocatalytic activities.[34–38] In this work, a series of Ag^+ doped–$ZnIn_{1.5}S_{3.25}$ samples were prepared, whose UV-vis diffuse reflectance spectra are given in Fig. 5. The absorption edge of the $ZnIn_{1.5}S_{3.25}$ solid solution is at about 490 nm, which shows an intense absorption band with a steep edge, indicating that the absorption is assigned to an intrinsic transition from the valence band to the conduction band of the solid solution and not the transition from impurity levels.[31] When the $ZnIn_{1.5}S_{3.25}$ solid solution is doped with Ag^+, its visible absorption is red-shifted from 490 to about 600 nm for Ag(3%)–$ZnIn_{1.5}S_{3.265}$. The absorption bands with tails are possibly ascribed to a discontinuous Ag4d level formed in the forbidden band. Besides, the Ag4d donor levels increase with the increase in the doping amounts from 0.5% to 3%, resulting in the slight decrease of the band gaps (shown in Table 2). There are no light

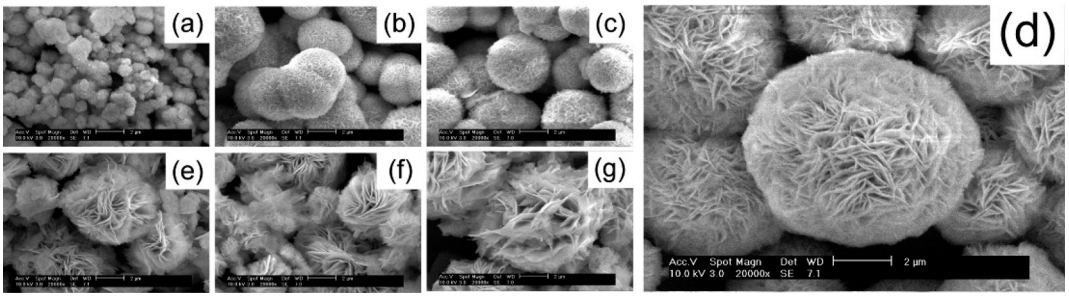

Fig. 3 SEM images of $ZnIn_{1.5}S_{3.25}$ samples prepared by adding different amounts of hydrochloric acid at 160 °C for 6 h. The amounts of hydrochloric acid are (a) 0 mL; (b) 0.25 mL; (c) 0.5 mL; (d) 1.0 mL; (e) 1.5 mL; (f) 2.0 mL; (g) 2.5 mL. The scale bar is 2 μm.

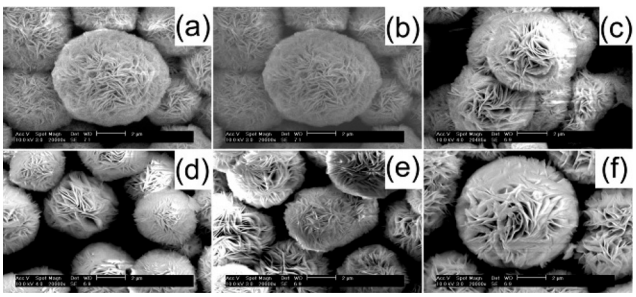

Fig. 4 SEM images of $Ag(y)–ZnIn_{1.5}S_{3.25+0.5y}$ samples prepared with different Ag^+ doping amounts at 160 °C for 6 h and adding 1 mL hydrochloric acid. The doping amounts are (a) 0; (b) 0.5%; (c) 1.0%; (d) 1.5%; (e) 2.0%; (f) 3.0%. The scale bar is 2 μm, and Fig. 4a is the same as Fig. 3d.

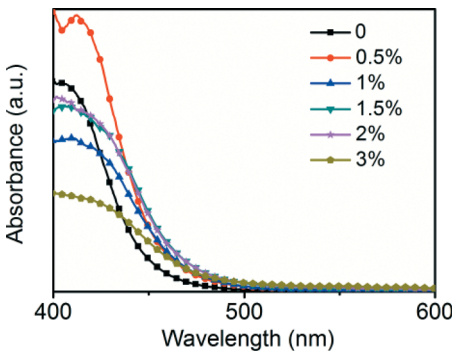

Fig. 5 UV-vis diffuse reflectance spectra of $Ag(y)–ZnIn_{1.5}S_{3.25+0.5y}$ samples prepared by adding 1 mL hydrochloric acid at 160 °C for 6 h.

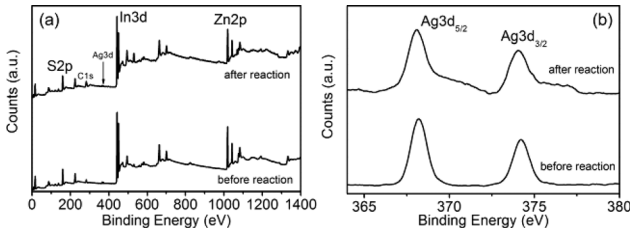

Fig. 6 XPS data collected before and after the photocatalytic H_2 evolution reaction for 15 hours from the surface of the $Ag(1.5\%)–ZnIn_{1.5}S_{3.2575}$ sample prepared by adding 1 mL hydrochloric acid at 160 °C for 6 h: (a) the survey spectra; (b) a partial spectra of the Ag3d core-level.

responses belonging to Ag_2S in the region longer than 550 nm for the doped solid solution, indicating the existence of Ag^+ as a dopant but not as Ag_2S.

XPS characterization of the $Ag(1.5\%)–ZnIn_{1.5}S_{3.2575}$ sample

Fig. 6a presents the XPS data of the $Ag(1.5\%)–ZnIn_{1.5}S_{3.2575}$ sample, showing the existence of Ag, In, Zn and S elements in the doped sample. The binding energies for $Ag3d_{5/2}$ and $Ag3d_{3/2}$ before the photocatalytic H_2 evolution reaction are 368.2 and 374.2 eV, respectively (as shown in Fig. 6b), indicating that the oxidation state of silver in the samples is Ag^+ which is in good agreement with that in the literature.[39] Therefore, the formula of Ag doped $ZnIn_xS_{1+1.5x}$ is given as $Ag(y)–ZnIn_xS_{1+1.5x+0.5y}$ for charge neutrality. Besides, the binding energies of In3d and Zn2p illustrate that their valence states are In^{3+} and Zn^{2+}, respectively (Fig. S5†). In addition, comparison of the samples before and after the photocatalytic reaction reveals that the binding energies of all the elements do not change, indicating that the doped solid solutions are quite stable in the presence of sacrificial reagents and under visible-light irradiation, and no obvious Ag^0/Ag^+ conversion happens. Moreover, to further ensure the doping position of Ag^+, the X-ray energy dispersive spectroscopy (XEDS) maps of silver, indium and zinc for the $Ag(1.5\%)–ZnIn_{1.5}S_{3.2575}$ sample were also investigated, as shown in Fig. S4.† The maps reveal that the distribution of all the cations are homogeneous, which further confirms the formation of the doped solid solution.

Photocatalytic activities

The effect of In/Zn molar ratios on the photocatalytic activities of $ZnIn_xS_{1+1.5x}$ solid solutions (synthetic conditions: hydrothermal reaction at 160 °C for 6 h, adding 1 mL hydrochloric acid) is evaluated in the presence of Ru (0.5 wt%) as the co-catalyst and Na_2S/Na_2SO_3 as sacrificial reagents under visible-light irradiation, as shown in Fig. 7. Pure ZnS has almost no hydrogen production. In^{3+} incorporation leads the activities of the $ZnIn_{0.8}S_{2.2}$ solid solution (x = 0.8) increasing to 0.45 mmol h^{-1} g^{-1}. The highest activity can reach 1.85 mmol h^{-1} g^{-1} for the sample $ZnIn_{1.5}S_{3.25}$ (x = 1.5). The increase of the photocatalytic activity is ascribed to an optimal band structure of $ZnIn_xS_{1+1.5x}$ solid solutions with a visible-light

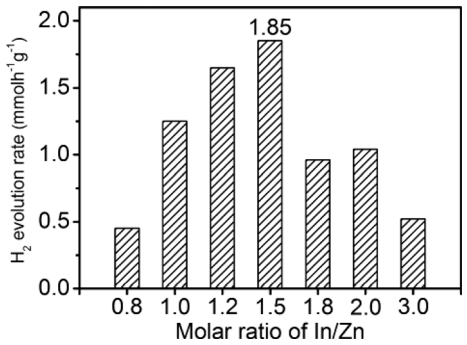

Fig. 7 H_2 evolution rates of as-prepared $ZnIn_xS_{1+1.5x}$ solid solution samples prepared by adding 1 mL hydrochloric acid at 160 °C for 6 h.

response and a negative conduction band level. However, the H_2 evolution rates decrease by further increasing the In^{3+} content. Although the light absorption range is expanded by reducing the band gap, the conduction band position is also lowered, which is unfavorable for water reduction. For comparison, the mixture of In_2S_3 and ZnS with the same atom ratio as the $ZnIn_{1.5}S_{3.25}$ sample exhibits only 0.22 mmol h^{-1} g^{-1} H_2 evolution rate under the same photocatalytic measurement, much lower than that of the $ZnIn_xS_{1+1.5x}$ solid solution. This further confirms the formation of the solid solution.

Table 1 presents the influence of different amounts of hydrochloric acid added, hydrothermal temperatures and hydrothermal reaction times on the photocatalytic activities of $ZnIn_{1.5}S_{3.25}$ samples. It is meaningful that the amount of hydrochloric acid added influences not only the crystal structure and the morphology of the solid solution, but also the photocatalytic activities. Without using hydrochloric acid before the hydrothermal reaction, the resultant sample had only a H_2 evolution rate of 0.36 mmol h^{-1} g^{-1}. After adding hydrochloric acid, the H_2 evolution rate increases intensely to as high as 1.85 mmol h^{-1} g^{-1}. Besides, when hydrothermal reactions were carried out in the range of 120–180 °C, the photocatalytic activities of the resultant samples are quite similar. However, upon further increasing the temperature to 200 °C, the photocatalytic activity decreases significantly. These phenomena are not the same as that reported by Chai and Peng who found that the pH value and the hydrothermal temperature had no such distinguished effects on the photocatalytic activities for H_2 generation.[30]

The H_2 evolution rates of $Ag(y)$–$ZnIn_{1.5}S_{3.25+0.5y}$ samples are shown in Table 2. All the doped samples can exhibit higher activities than that of the undoped sample, indicating the positive effect of Ag^+ doping on the photocatalysts. In the meantime, the H_2 evolution rates are sensitive to the Ag^+ doping amount. When 0.5% Ag^+ is introduced, the H_2 evolution rate dramatically increases to 2.81 mmol h^{-1} g^{-1}. Upon further increasing the doping amounts, the H_2 evolution rate can reach a maximum value of 3.20 mmol h^{-1} g^{-1} for the $Ag(1.5\%)$–$ZnIn_{1.5}S_{3.2575}$ sample. In fact, quaternary Ag–In–Zn–S was studied previously. In our work, a 3.20 mmol h^{-1} g^{-1} hydrogen evolution rate was obtained for $Ag(1.5\%)$–$ZnIn_{1.5}S_{3.2575}$

Table 2 Influence of the compositions and band gaps on the photocatalytic activities of the $Ag(y)$–$ZnIn_{1.5}S_{3.25+0.5y}$ samples

Sample/y^a	Band gap^b/eV	H_2 evolution rate^c/mmol h^{-1} g^{-1}
0	2.64	1.85
0.5%	2.57	2.81
1.0%	2.48	2.94
1.5%	2.47	3.20
2.0%	2.45	2.58
3%	2.41	1.94

[a] Calculated from the atomic ratio of the $Ag^+/(In^{3+} + Zn^{2+})$ in the starting materials. [b] The band gaps are calculated using a $(Ahv)^{1/2}$–hv plot based on the absorbance of the UV-vis DRS. [c] Catalysts, 0.1 g; reactant solution, 100 mL aqueous solution containing 0.35 M Na_2S and 0.25 M Na_2SO_3 as sacrificial reagents with 0.5 wt% Ru loaded as the co-catalyst; light source, a 300 W xenon lamp with a cut-off filter ($\lambda \geq 420$ nm); the H_2 evolution rates are calculated using the average rate in the first five hours.

Table 1 Summary of the amounts of added hydrochloric acid, hydrothermal temperatures, hydrothermal reaction times and photocatalytic activities of $ZnIn_{1.5}S_{3.25}$ solid solution photocatalysts

HCl/mL	Hydrothermal temperature/°C	Reaction time/h	H_2 evolution rate^a/mmol h^{-1} g^{-1}
0	160	6	0.36
0.25	160	6	0.71
0.5	160	6	0.94
1.0	160	6	1.85
1.5	160	6	0.96
2	160	6	0.92
2.5	160	6	0.79
1.0	200	6	0.75
1.0	180	6	1.70
1.0	140	6	1.83
1.0	120	6	1.76
1.0	160	3	0.60
1.0	160	9	1.44

[a] Catalysts, 0.1 g; reactant solution, 100 mL aqueous solution containing 0.35 M Na_2S and 0.25 M Na_2SO_3 as sacrificial reagents with 0.5 wt% Ru loaded as the co-catalyst; light source, a 300 W xenon lamp with a cut-off filter ($\lambda \geq 420$ nm); the H_2 evolution rates are calculated using the average rate of the first five hours.

whereas 0.80 mmol h^{-1} g^{-1} was obtained for $(AgIn)_{0.22}Zn_{1.56}S_2$ in Kudo's classic work.[31] Obviously, the detailed compositions will strongly influence the photocatalytic activity.

As we know, metal ion doping is a very important strategy in photocatalysis, especially in photocatalytic water splitting. Currently, two possible mechanisms are suggested to explain the photocatalytic process. The first one is that metal ion dopants create donor levels in the forbidden band of the photocatalysts, which can expand the range of light absorption.[31,32] That is to say, additional photogenerated electron transitions happen from the donor levels to the conduction band of the photocatalysts. In our work, Ag4d donor levels are supposed to be created above the valence band of the $ZnIn_xS_{1+1.5x}$ solid solution from which the electrons can be photoexcited to the conduction band, as shown in Fig. 8a. Therefore, the photocatalytic activities are enhanced in this way. The second mechanism is that the donor levels contributed by the doping ions can trap the photogenerated holes and facilitate charge separation and transfer.[38,40] Therefore, all the doped samples exhibit higher H_2 evolution rates than those of the undoped samples.

In order to find which mechanism may play a key role in our photocatalyst systems, the dependence of H_2 evolution rates of Ag(1.5%)–$ZnIn_{1.5}S_{3.2575}$ on the wavelengths of the different cut-off filters was investigated, as shown in Fig. 8b. The H_2 evolution rates obtained with 420 and 455 nm cut-off filters are 3.20 and 1.68 mmol h^{-1} g^{-1}, respectively, whereas the H_2 evolution rates for 495 nm, 550 and 590 nm cut-off filters are only 0.15, 0.005 and 0 mol h^{-1} g^{-1}, respectively. These results reveal that the enhancement of H_2 evolution rates by Ag^+ doping mainly takes place in the short-wavelength range (≤495 nm), close to the intrinsic absorption region of the $ZnIn_{1.5}S_{3.25}$ solid solution. Therefore, it is believed that the enhancement is primarily ascribed to the promotion of the photogenerated charge separation and transfer in the intrinsic absorption region of the Zn–In–S solid solution. Besides,

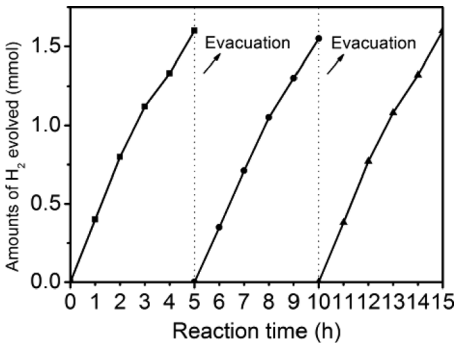

Fig. 9 Stability test of the Ag(1.5%)–$ZnIn_{1.5}S_{3.2575}$ sample prepared by adding 1 mL hydrochloric acid at 160 °C for 6 h.

the onset of the action spectrum of the H_2 evolution rate is consistent with the diffuse reflectance spectrum, indicating that Ag4d donor levels participate in the formation of the energy structure of the doped solid solution and the visible light absorption of the photocatalyst comes from the transition between the Ag4d donor levels and the conduction band of the solid solution.[41,42] Besides, the Ag(1.5%)–$ZnIn_{1.5}S_{3.2575}$ solid solution exhibits good stability, as shown in Fig. 9. The doped sample can show quite stable H_2 evolution activity without obvious decrease in the first three cycles. The slight drop in the H_2 evolution rate may be due to the consumption of the sacrificial reagents in the three reaction cycles.[30]

Conclusions

In summary, two series of $ZnIn_xS_{1+1.5x}$ solid solutions and Ag(y)–$ZnIn_xS_{1+1.5x+0.5y}$ solid solutions are prepared by hydrothermal methods. The photocatalytic H_2 evolution rates are greatly influenced by the synthetic conditions of the photocatalysts, such as the In/Zn molar ratios, the amount of hydrochloric acid added before the hydrothermal reaction, the hydrothermal temperature and the reaction time. A 1.85 mmol h^{-1} g^{-1} H_2

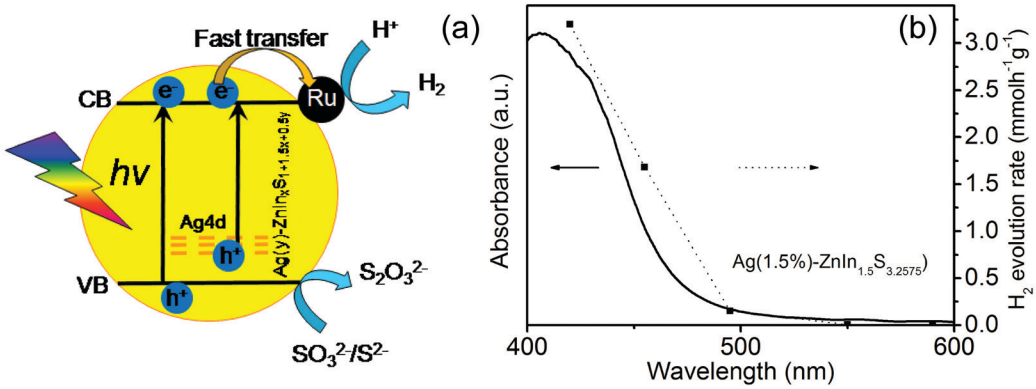

Fig. 8 (a) The mechanism of water reduction to H_2 evolution and sacrificial reagent oxidation on the surface of the Ag(y)–$ZnIn_xS_{1+1.5x+0.5y}$ solid solutions; (b) dependence of the H_2 evolution rates on the wavelengths of the cut-off filter for the Ag(1.5%)–$ZnIn_{1.5}S_{3.2575}$ sample. Reaction conditions: 0.1 g of Ag(1.5%)–$ZnIn_{1.5}S_{3.2575}$ sample prepared by adding 1 mL hydrochloric acid at 160 °C for 6 h in a 100 mL aqueous solution containing 0.35 M Na_2S and 0.25 M Na_2SO_3 as sacrificial reagents with 0.5 wt% Ru loaded as the co-catalyst, a 300 W xenon lamp with different cut-off filters ($\lambda \geq 420$ nm, 455 nm, 495 nm, 550 nm, 590 nm). The H_2 evolution rates are calculated using the average rate of the first three hours, with 0.5 wt% Ru loaded as the co-catalyst.

evolution rate is obtained for the $ZnIn_{1.5}S_{3.25}$ solid solution, which is based on In/Zn molar ratio of 1.5 and preparation at 160 °C for 6 h by adding 1 mL hydrochloric acid before the hydrothermal reaction. Further Ag^+ doping can result in a higher H_2 evolution rate of 3.20 mmol h^{-1} g^{-1} for the Ag(1.5%)–$ZnIn_{1.5}S_{3.2575}$ sample. This work provides a new opportunity to develop novel and efficient photocatalysts by transition metal ion doping.

Acknowledgements

This work was financially supported by the National Natural Science Foundation of China (21173260, 51072221 and 91233202), the Knowledge Innovation Program of the Chinese Academy of Sciences and the National Basic Research Program of China (973 project, 2012CB932903 and 2012CB932904).

Notes and references

1 A. Fujishima and K. Honda, *Nature*, 1972, **238**, 37.
2 N. S. Lewis, *Nature*, 2001, **414**, 589.
3 Z. Zou, J. Ye, K. Sayama and H. Arakawa, *Nature*, 2001, **414**, 625.
4 K. Maeda, K. Teramura, D. Lu, T. Takata, N. Saito, Y. Inoue and K. Domen, *Nature*, 2006, **440**, 295.
5 H. Kato, K. Asakura and A. Kudo, *J. Am. Chem. Soc.*, 2003, **125**, 3082.
6 M. Matsumura, Y. Saho and H. Tsubomura, *J. Phys. Chem.*, 1983, **87**, 3807.
7 N. Bao, L. Shen, T. Takata and K. Domen, *Chem. Mater.*, 2008, **20**, 110.
8 H. Yan, J. Yang, G. Ma, G. Wu, X. Zong, Z. Lei, J. Shi and C. Li, *J. Catal.*, 2009, **266**, 165.
9 R. Williams, *J. Chem. Phys.*, 1960, **32**, 1505.
10 G. Chen, D. Li, F. Li, Y. Fan, H. Zhao, Y. Luo, R. Yu and Q. Meng, *Appl. Catal., A*, 2012, **443–444**, 138.
11 G. Chen, F. Li, Y. Fan, Y. Luo, D. Li and Q. Meng, *Catal. Commun.*, 2013, **40**, 51.
12 Y. Wang, Y. Wang and R. Xu, *J. Phys. Chem. C*, 2013, **117**, 783.
13 Y. Fan, G. Chen, D. Li, F. Li, Y. Luo and Q. Meng, *Mater. Res. Bull.*, 2011, **46**, 2338.
14 J. Hou, C. Yang, H. Cheng, Z. Wang, S. Jiao and H. Zhu, *Phys. Chem. Chem. Phys.*, 2013, **15**, 15660.
15 J. Hou, C. Yang, Z. Wang, S. Jiao and H. Zhu, *RSC Adv.*, 2012, **2**, 10330.
16 T.-H. Yu, W.-Y. Cheng, K.-J. Chao and S.-Y. Lu, *Nanoscale*, 2013, **5**, 7356.
17 S.-W. Cao, Y.-P. Yuan, J. Fang, M. M. Shahjamali, F. Y. C. Boey, J. Barber, S. C. Joachim Loo and C. Xue, *Int. J. Hydrogen Energy*, 2013, **38**, 1258.
18 Z. Lei, W. You, M. Liu, G. Zhou, T. Takata, M. Hara, K. Domen and C. Li, *Chem. Commun.*, 2003, 2142.
19 N. S. Chaudhari, A. P. Bhirud, R. S. Sonawane, L. K. Nikam, S. S. Warule, V. H. Rane and B. B. Kale, *Green Chem.*, 2011, **13**, 2500.
20 J. Zhou, G. Tian, Y. Chen, X. Meng, Y. Shi, X. Cao, K. Pan and H. Fu, *Chem. Commun.*, 2013, **49**, 2237.
21 Y. Li, J. Wang, S. Peng, G. Lu and S. Li, *Int. J. Hydrogen Energy*, 2010, **35**, 7116.
22 B. Chai, T. Peng, P. Zeng and X. Zhang, *Dalton Trans.*, 2012, **41**, 1179.
23 S. Shen, X. Chen, F. Ren, C. X. Kronawitter, S. S. Mao and L. Guo, *Nanoscale Res. Lett.*, 2011, **6**, 290.
24 X. Bai and J. Li, *Mater. Res. Bull.*, 2011, **46**, 1028.
25 Y. Chen, S. Hu, W. Liu, X. Chen, L. Wu, X. Wang, P. Liu and Z. Li, *Dalton Trans.*, 2011, **40**, 2607.
26 J. Shen, J. Zai, Y. Yuan and X. Qian, *Int. J. Hydrogen Energy*, 2012, **37**, 16986.
27 D. Jing, M. Liu and L. Guo, *Catal. Lett.*, 2010, **140**, 167.
28 S. Shen, L. Zhao, Z. Zhou and L. Guo, *J. Phys. Chem. C*, 2008, **112**, 16148.
29 J. F. Reber and M. Rusek, *J. Phys. Chem.*, 1986, **90**, 824.
30 B. Chai, T. Peng, P. Zeng, X. Zhang and X. Liu, *J. Phys. Chem. C*, 2011, **115**, 6149.
31 I. Tsuji, H. Kato, H. Kobayashi and A. Kudo, *J. Am. Chem. Soc.*, 2004, **126**, 13406.
32 I. Tsuji, H. Kato and A. Kudo, *Chem. Mater.*, 2006, **18**, 1969.
33 R. Shannon, *Acta Crystallogr., Sect. A: Cryst. Phys., Diffr., Theor. Gen. Crystallogr.*, 1976, **32**, 751.
34 F. Li, G. Chen, J. Luo, Q. Huang, Y. Luo, Q. Meng and D. Li, *Catal. Sci. Technol.*, 2013, **3**, 1993.
35 Y. Li, G. Chen, C. Zhou and J. Sun, *Chem. Commun.*, 2009, 2020.
36 Y. Wang, J. Wu, J. Zheng, R. Jiang and R. Xu, *Catal. Sci. Technol.*, 2012, **2**, 581.
37 K. Ikeue, S. Shiiba and M. Machida, *ChemSusChem*, 2011, **4**, 269.
38 K. Ikeue, Y. Shinmura and M. Machida, *Appl. Catal., B*, 2012, **123–124**, 84.
39 B. V. R. Chowdari, K. F. Mok, J. M. Xie and R. Gopalakrishnan, *J. Non-Cryst. Solids*, 1993, **160**, 73.
40 M. A. Fox and M. T. Dulay, *Chem. Rev.*, 1993, **93**, 341.
41 H. Zhang, G. Chen, X. He and Y. Li, *Int. J. Hydrogen Energy*, 2012, **37**, 5532.
42 I. Tsuji, Y. Shimodaira, H. Kato, H. Kobayashi and A. Kudo, *Chem. Mater.*, 2010, **22**, 1402.

